

Understanding Electrochemical Intercalation of Al^{3+} Cation into the WO_3 Electrochromic Electrode from Solid Electrolyte Interphase and Mass Changes

Sheng Liu, Hongliang Zhang,* Xin Zhang, Qiang Wang, Chengli Zhang, Ran Jiang, Junhua Gao, Lingyan Liang, and Hongtao Cao



Cite This: *ACS Appl. Energy Mater.* 2022, 5, 1833–1839



Read Online

ACCESS |



Metrics & More



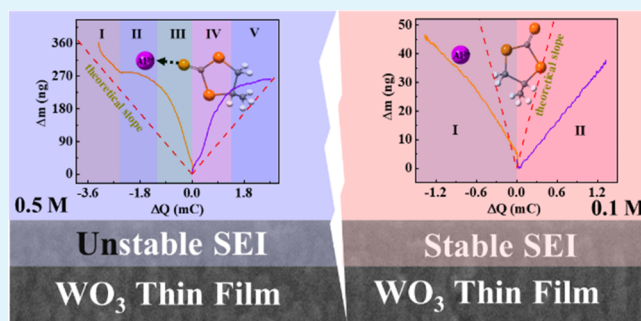
Article Recommendations



Supporting Information

ABSTRACT: Multivalent chemistry has drawn extensive research interests because it provides intriguing benefits to develop beyond-lithium-ion electrochromic and energy storage technologies. Among the multivalent candidates, the aluminum (Al)-based electrolyte offers an attractive high capacity for designing multivalent-ion electrochromic batteries and devices. However, the understanding of complex electrochemical and mechanical interactions of the electrode/electrolyte interface during cycling is extremely limited. Herein, we develop an Al^{3+} -based half-cell that consisted of a WO_3 thin film cathode, $\text{Al}(\text{ClO}_4)_3\text{-PC}$ electrolyte, and Au counter electrode. Electrochemical quartz crystal microbalance (EQCM) observations suggest that there is a link between the interfacial degradation of WO_3 /electrolyte and the formation of chelate-like compounds in a high-concentration electrolyte environment. The intercalation/de-intercalation of the Al^{3+} cations in WO_3 electrodes was directly evaluated through in situ real-time EQCM. As indicated by the results of EQCM, the formation of chelate-like compounds leads to the irreversible process of intercalation and de-intercalation in the WO_3 thin film electrode and the instability of the solid electrolyte interphase. The validated EQCM-based analysis provides a correlation between solution concentration and cycle stability, which would be expected to reveal new insights into the electrochemical and electrochromic behavior in many other multivalent systems.

KEYWORDS: solid electrolyte interphase, electrochemical quartz crystal microbalance, chelate-like compounds, cyclic stability, Al-ion intercalation



1. INTRODUCTION

Within a few decades, batteries with high energy density and superior cycling life have attracted much more attention than ever. Multivalent-ions like Zn, Mg, and Al could be potential candidates owing to their attributes such as environmentally benign, high power capability, and safety. Currently, there are two natural advantages currently being accepted in the research of Al-ion electrolytes. One is that the Al^{3+} -based electrolyte possesses higher volumetric capacity than that of Li or Mg.¹ The other is that more electrons can be injected into the host framework, further improving the coloration contrast in the electrode of the Al-ion electrolyte.² It is a notable example for an aluminum metal anode, and a three-dimensional graphitic-foam cathode is a rechargeable aluminum battery with high rate capacity.³ Recently, Li et al. have developed an aqueous hybrid $\text{Zn}^{2+}/\text{Al}^{3+}$ electrochromic battery.⁴ Although Al^{3+} has a remarkably high capacity of 2980 mAh/g in its native state,⁵ little is known about the intercalation/de-intercalation and its electrochemical stability after the so-called “aluminumization”. Degradation of electrode materials often occurs during the

intercalation/de-intercalation cycles due to the complex electrochemical and mechanical interactions.

To find a solution to mitigating the electrochemical failure, it is essential to obtain a fundamental understanding for the electrochemical instability in the electrode active interface during cycling. In this context, a number of in situ techniques have been developed to follow the characteristic evolution of electrode active interfaces including optical microscopy, X-ray diffraction (XRD), transmission electron microscopy (TEM), atomic force microscopy, and electrochemical quartz crystal microbalance (EQCM).^{6–8} Among them, in situ EQCM observation is a powerful tool to understand the local collective mass changes for the complex electrochemical and mechanical

Received: October 16, 2021

Accepted: January 14, 2022

Published: January 26, 2022



interactions during cycling. For instance, a composite electrode model in the Li-ion electrolyte has been investigated by EQCM.⁹ By using EQCM technology, it has been verified that the desolvation of the monovalent Na-ion still should be required during the discharge process.¹⁰ Commonly, redox reactions are easily hindered by the formation of a complicated interface known as the solid electrolyte interphase (SEI).¹¹ The formation of an ionically permeable SEI layer has been confirmed in the Zn²⁺-based electrolyte/electrode interface in previous literature.¹² However, as far as we know, in situ EQCM has not been performed during the investigation of the Al³⁺-based electrolyte for electrochromic batteries or devices. In situ EQCM could be an important method to verify the key factors, considering the degradation mechanism of the electrode/electrolyte interface.

In this article, we develop a novel Al-ion half-cell consisting of a WO₃ thin film cathode, Al(ClO₄)₃-PC electrolyte, and Au counter electrode. The deterioration mechanism of a WO₃ thin film cathode has been depicted according to the experimental results as listed below. In situ EQCM observation reveals that Al³⁺-based chelate-like compounds appeared at the active interface of WO₃/electrolyte in high-concentration solutions, as depicted in Figure 1. The stability of SEI will be affected by

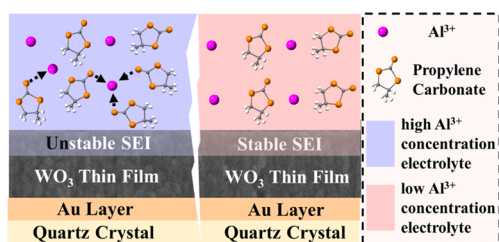


Figure 1. Schematic depiction of the influence of aluminum ion concentration on the stability of the SEI layer.

the appearance of chelate-like compounds because the chelate-like compounds can inhibit the process of intercalation and deintercalation in the WO₃ thin film electrode.

2. EXPERIMENTAL METHODS

2.1. Preparation of Thin Films. The WO₃ thin films were deposited on gold-patterned quartz substrates by an electron beam evaporation technique (MUE-ECO made in ULVAC, Japan). By using an electron beam of 10 kV, evaporation was performed in a high-vacuum of less than 5×10^{-3} Pa, with a substrate temperature of 200 °C. The thickness of the WO₃ thin film was set to be 300 nm (~350 nm measured by SEM in Figure S1) with a deposition rate of 0.10–0.20 nm/s. Aluminum perchlorate nonahydrate (Al(ClO₄)₃·9H₂O, 99%) (J&K Scientific) was also used with a molar ratio from 1:100 to 1:2 in propylene carbonate (PC, 99%) (Sinopharm Chemical Reagent Co., Ltd.) solvent.

2.2. Measurements. Micro-FTIR spectroscopy (μ -FTIR, Cary660 + 620, Agilent, Santa Clara, CA, USA) was used for the Fourier transform infrared resonance (FT-IR) spectrum in the attenuated total reflectance (ATR) mode in the range of 500 to 4000 cm⁻¹. The resolution was 2 cm⁻¹, and the spectrum of each specimen was scanned more than 32 times. The electrochemical performances of the WO₃ thin films were recorded by using a potentiostat (PGSTAT 204, Autolab, Eco-Chemie, The Netherlands). For the EQCM tests, a 6 MHz gold-patterned quartz substrate was deposited with a WO₃ thin film as the working electrode. Typically, the thickness and diameter of the metal layer were 100 nm and 6.6 mm, respectively. A Au wire and a Ag/AgCl served as the counter electrode and the reference electrode, respectively. The electro-

chemical experiments were performed in the 0.1 and 0.5 M Al(ClO₄)₃-PC electrolyte. The electrolyte volume was about 5 mL. The EQCM equipment was turned on 1 h before the measurements to stabilize the frequency signals. Cyclic voltammetry (CV) and galvanostatic charge–discharge (GCD) were carried out on the EQCM equipment. All the electrochemical measurements were performed in the cell reaction tank on the optical shock absorption platform at room temperature.

2.3. Theory and Calculations. Based on the following Sauerbrey equation, the mass change (Δm , g) was calculated directly from the resonator frequency change (Δf , Hz) by the EQCM:

$$\Delta m = -\frac{\sqrt{\rho_q \mu_q}}{2f_0} \cdot \Delta f \quad (1)$$

where ρ_q , μ_q , and f_0 are the density of quartz (2.648 g cm⁻³), the shear modulus of quartz (2.947×10^{11} g cm⁻¹ s⁻²), and the resonant frequency of the fundamental mode of the loaded crystal (Hz), respectively.¹³ Thus, EQCM made it possible to measure the mass change of the WO₃ thin films deposited on the quartz resonator.¹⁴

The data recorded by CV were calculated according to Faraday's law. This method allowed the results with the theoretical mass change as a function of comparing the charge in the so-called mass to charge ratio diagram:

$$\Delta m = \frac{\Delta Q \cdot M}{F \cdot z} \quad (2)$$

where ΔQ , M , F , and z are the charge exchanged (C), the molecular weight of the insertion/extraction ion (g mol⁻¹), the Faraday's constant (96,485 C mol⁻¹), and the valence number of the insertion/extraction ions, respectively.¹⁵

3. RESULTS AND DISCUSSION

3.1. Ion–Molecule Interactions in Al(ClO₄)₃-PC Solutions. Figure 2a–c shows the FT-IR absorption spectra of the pure PC solvent without Al(ClO₄)₃ salt and the PC solutions with different concentrations of Al(ClO₄)₃ salt. The absorption peaks at around 710, 773, 1038, 1173, and 1780 cm⁻¹ marked by the vertical dotted lines are attributed to the intrinsic vibration modes of the pure PC solvent. Among them, the peaks at 710 and 773 cm⁻¹ confirm the ring deformation. In addition, the peaks at 1038 and 1173 cm⁻¹ are due to the C–O–C stretching mode. Another peak at 1780 cm⁻¹ can be identified as the C=O stretch.¹⁶ It is observed that the IR frequency shifts of these vibration peaks depend on the different concentrations of Al(ClO₄)₃ salt in the PC solutions. The increase in the intensity of the ring deformation peak (Figure 2a) can be attributed to the increase of the fraction of the ring deformation.^{17,18} The large shift to shorter wave lengths in the C–O–C vibration peaks (Figure 2b) (blue shift) is shown to be mainly due to the Al bonding of the electrons by the hydroxylic solvent (PC),¹⁹ which causes a heightening of the C–O bonds. This blue shift is expected when the electron lone pairs of the O atoms from the PC molecule are used to form bonds with the Al³⁺ metallic ions, as shown in Figure 2d. Moreover, the spectral peak at 1038 cm⁻¹ of the C–O–C stretching is perturbed, forming a shoulder that often appears in such FT-IR vibrational spectra of the different concentrations of Al(ClO₄)₃ salt in the PC solutions. It can be suggested that there is a strong interaction between the Al³⁺ and PC molecules because the newly formed Al–O bond affects the C atoms in the PC molecule.²⁰ This interaction occurs mainly on the carbonyl oxygen atom and the ring of the PC molecule. The above analysis initially confirms the complexation of Al(ClO₄)₃ with PC. Figure 2c reveals that there has been a marked increase (blue shift) in the

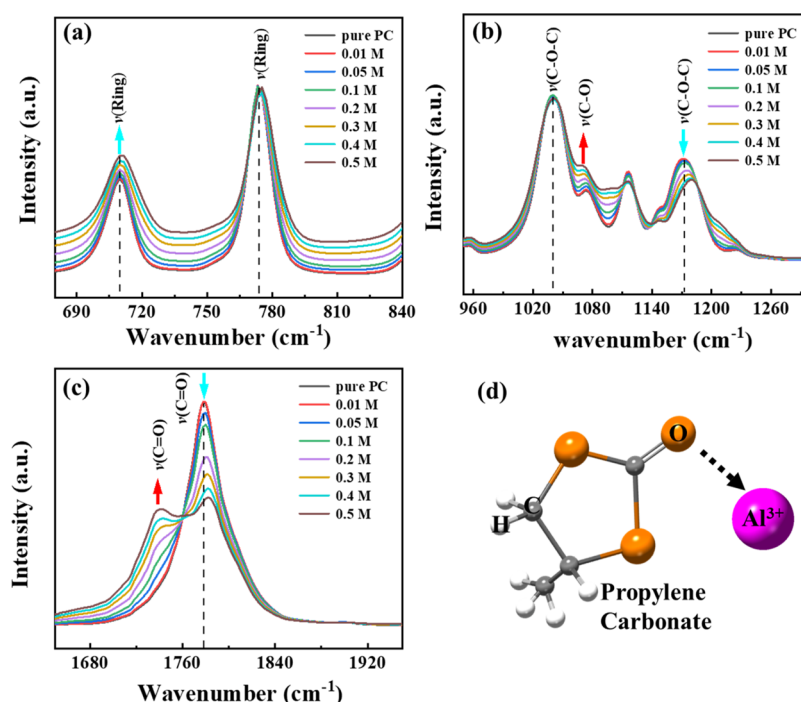


Figure 2. (a–c) Evolution of the FT-IR spectrum upon increasing the $\text{Al}(\text{ClO}_4)_3$ salt concentration. The vertical-dotted lines show the peak positions in pure PC solvent. As the concentration increases, the color of the arrow represents the red/blue shift, and the direction represents the increase/decrease of peak intensity. (d) Schematic indicating the strong interaction between the Al^{3+} ion and PC solvent.

wavenumber of the $\text{C}=\text{O}$ stretch after introducing $\text{Al}(\text{ClO}_4)_3$ into PC. Moreover, the half-peak breadth of the $\text{C}=\text{O}$ stretch increases significantly with the increase of the $\text{Al}(\text{ClO}_4)_3$ concentration in PC, whereas a shoulder peak at 1739 cm^{-1} is gradually formed on the lower wavenumber side. Simultaneously, the intensity of the shoulder peak gradually increases with the increase of the $\text{Al}(\text{ClO}_4)_3$ concentrations, especially for the 0.4 and the 0.5 M $\text{Al}(\text{ClO}_4)_3$ -PC solutions. The spectra for the IR at 1780 cm^{-1} exhibit a significant fluctuation, which originates from a strong interaction between the Al^{3+} cations and PC molecules through the oxygen atom of the carbonyl group. Besides, the peak at 1120 cm^{-1} is due to the swing and bending of the $\text{C}-\text{H}$.¹⁷ Based on the FT-IR observations, it can be concluded that the Al ions can exist in a free state at low concentrations and form strong interactions with the PC molecules as the concentrations increase and can even form chelate-like compounds with PC molecules at high concentrations. Thus, the 0.1 and 0.5 M $\text{Al}(\text{ClO}_4)_3$ -PC solutions are selected as the typical electrolyte to consider the intercalation and de-intercalation mechanism of aluminum ions in WO_3 thin films via EQCM below.

3.2. Electrochemical Quartz Crystal Microbalance.

Figure 3 displays the EQCM curves of the samples stepped between -0.2 and $+0.8\text{ V}$ at a scan rate of 50 mV/s in the 0.1 and 0.5 M $\text{Al}(\text{ClO}_4)_3$ -PC (CV in 0.02 and 0.05 M $\text{Al}(\text{ClO}_4)_3$ -PC can be seen in **Figure S2**). Due to the intercalation of the Al^{3+} ions during the reduction bias (coloration) process, the mass response shows an upward trend (the blue curve in **Figure 3a**). In the reverse process, the inserted species are de-intercalated from the WO_3 film during the oxidation bias (bleaching), resulting in a decrease of the electrode mass.²¹ By comparing the de-intercalation formal potentials of the two concentrations of 0.1 and 0.5 M $\text{Al}(\text{ClO}_4)_3$ -PC solution, a shift of $\sim 30\text{ mV}$ could be observed based on the Nernst equation²² if Al^{3+} is the charge-compensating ion. In contrast, a larger

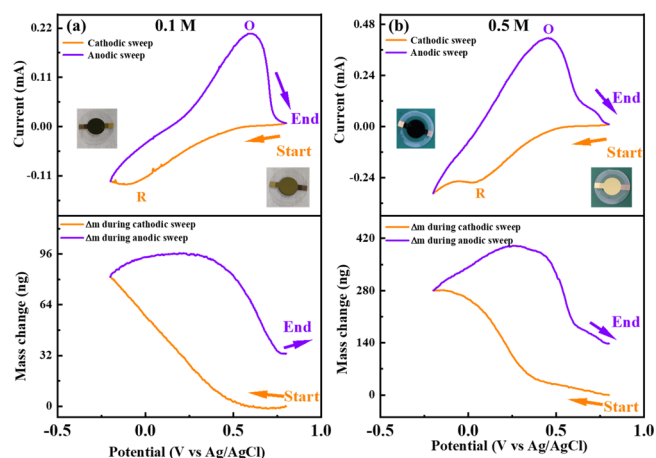


Figure 3. (a–b) CV curves of the WO_3 electrode at a scan rate of 50 mV/s (top) and the EQCM results of the WO_3 (bottom) in 0.1 and 0.5 M. Orange, cathodic scan; purple, anodic scan. R: reduction peak position; O: oxidation peak position. Inset: digital photos of WO_3 in bleaching or coloration states.

potential transition is obtained in the high-concentration solution, indicating that the counterions are also involved in the charge compensation process.²³ In addition, a slight increase in the mass change curve is noted at the beginning of the discharge process. Previous observations suggest that during the discharge process, the cations deeply confined in the micropores/nanopores undergo a charge transfer process to the wider pores before being released.²⁴ It should be noted that the net mass gain between the reduction and oxidation processes for the 0.5 M $\text{Al}(\text{ClO}_4)_3$ -PC is $138 \pm 0.3\text{ ng}$, being larger than that for the 0.1 M $\text{Al}(\text{ClO}_4)_3$ -PC of $33.2 \pm 0.3\text{ ng}$. There are two probable causes for the differences between the two concentrations of solutions. One possible implication is

that the more intense electrochemical activity of 0.5 M $\text{Al}(\text{ClO}_4)_3\text{-PC}$ can allow more Al-ions to be intercalated/de-intercalated. The chelate-like compounds are another potential component. High-concentration solutions are more prone to the formation of chelate-like compounds, which affects the electrode/electrolyte interface stability significantly.²⁵

Figure 4 presents the CV curves and mass change plots measured at 0.1 and 0.5 M with a scan rate of 50 mV/s

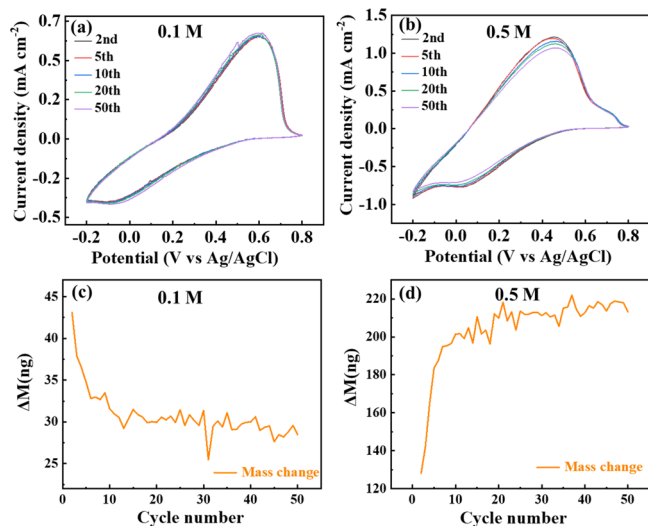


Figure 4. (a–b) Cyclic voltammograms (CVs) at the scan rate of 50 mV/s and (c–d) mass change during 50 cycles in 0.1 and 0.5 M.

between -0.2 and $+0.8$ V during the first 50 cycles. The essentially identical CV curves of the 0.1 M (Figure 4a) indicate its reversible redox reaction. In contrast, the CV curves of the 0.5 M reveal a continuous decrease in electroactivity (Figure 4b). Correspondingly, Figure 4c,d shows the simultaneous mass change corresponding to each CV scan. After the 50 repeated scans, the mass accumulation of the samples in 0.1 and 0.5 M $\text{Al}(\text{ClO}_4)_3\text{-PC}$ solutions is estimated to be 1.5 and 10 μg , respectively. This discrepancy can be partially attributed to the presence of trapped ions (Al^{3+} , ClO_4^- , and PC molecule) in the WO_3 thin film, which could lead to the change of crystallinity.^{26,27} A novel in situ TEM has been demonstrated to identify the WO_3 irreversible transformation to nanocrystalline Li_2WO_4 in our previous work.²⁸ Another noteworthy aspect of the interface degradation is SEI.^{6,29,30} The formation and stability of the dynamic SEI are essential to prevent the rapid capacity decay and continuous consumption of the electrolyte.³¹ In terms of our electrode/electrolyte system, the initial 10 electrochemical cycles are the essence of the SEI formation process where the SEI layer is well adhered to the electrode. The SEI layer could prevent further electrolyte decomposition and maintains the continued CV cycles for the $\text{Al}(\text{ClO}_4)_3\text{-PC}$ electrolyte, similar to those reported in previous work.³² To further elucidate the role of the chelate-like compounds on the active interface of the WO_3 electrode and Al^{3+} -based electrolyte, the microstructure and morphology of the as-deposited and electrochemically cycled WO_3 thin films were investigated by SEM, TEM, and XRD, as seen in Figures S3–S5. The SEM results in Figure S3 show that damage of the WO_3 thin film cycled under the high-concentration (0.5 M) electrolyte is more severe than that under the low-concentration (0.1 M) electrolyte. A

possible reason is that the stable SEI layer buffers impact the intercalation and de-intercalation in the WO_3 thin film electrode under the low-concentration (0.1 M) electrolyte. Examination of the electrode–electrolyte interface most often requires further TEM imaging examinations to confirm the SEI layers. The morphological differences of the SEI layer on the electrochemically cycled WO_3 electrodes in the 0.1 and 0.5 M $\text{Al}(\text{ClO}_4)_3\text{-PC}$ electrolyte are observed in Figure S4b,c, respectively. The SEI layer on the WO_3 thin film cycled under the low-concentration (0.1 M) electrolyte is more complete and continuous than that under the high-concentration (0.5 M) electrolyte. It is believed that the intact and uniform SEI layer on the WO_3 electrode cycled under the low-concentration electrolyte can stabilize the structure of the intercalation electrode material.³³ The accumulation of mass during the GCD also verifies this point of view (Figures S6 and S7). The case of the WO_3 thin film is very interesting because the initial decrease in capacity retention is related to a larger irreversible capacity in several initial cycles. In the subsequent cycles, the quality of SEI is improved, and the irreversibility of the capacity is reduced, which stabilizes the capacity retention. This conclusion is further evidenced in the literature for multivalent complex transfer through the electrode/electrolyte interface.³⁴ The physical properties of the SEI may be significantly affected as the concentration of chelate-like compounds increases,^{35,36} in our opinion, namely, its thickness and porosity.³⁷ In an ideal case, the SEI prevents further degradation of the electrolyte by blocking the electron transport through it while the Al-ions shuttle back and forth in the WO_3 electrode. When a large amount of chelate-like compounds is present, it could destroy the balance of the SEI film and affect the stability of the interface,³⁸ as depicted in Figure 1. It is worth pointing out that the optimized 0.1 M $\text{Al}(\text{ClO}_4)_3\text{-PC}$ electrolyte has the ability to build highly reversible aluminum-ion ESSDs with a high coloration efficiency of $102.2 \text{ cm}^{-1} \text{ C}^{-1}$ and an excellent long-term cycling stability of over 10,000 cycles in our previous work.³⁹

Figure 5a,b shows the electrode mass change vs charge during the polarization of the WO_3 thin films in the 0.1 and 0.5

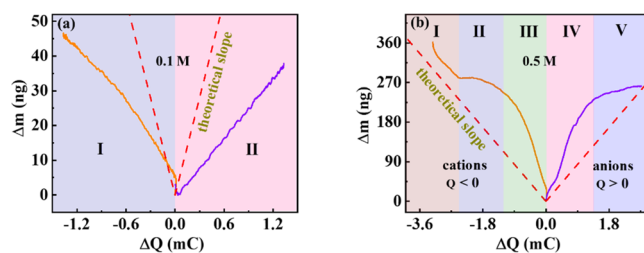


Figure 5. Relationship between electrode mass change and charge of the WO_3 thin films in (a) 0.1 and (b) 0.5 M $\text{Al}(\text{ClO}_4)_3\text{-PC}$ electrolyte. Red-dotted lines are the theoretical mass change of pure Al-ion calculated from the Faraday's law.

M $\text{Al}(\text{ClO}_4)_3\text{-PC}$ electrolyte, respectively. The definition of the red dotted line can vary depending on Faraday's law.¹⁵ If strictly involving one species, the $F \times \frac{\Delta m}{\Delta q}$ function should theoretically be equivalent to the molecular weight of the species intercalated/de-intercalated. In contrast, these experimental values are actually the average mass of the materials involved in the electrochemical reaction. According to Figure 5a, it is considered that the Al^{3+} , ClO_4^- , and PC molecules are

adsorbed to balance the negative or positive charges on the surface of the WO_3 film. What can be obviously seen in Table S1 are the lower values of the experimental average molar weight of the adsorbed species than a theoretical possibility (9 g/mol). Obviously, species such as heavier ClO_4^- ions and PC molecules are believed to be a significant contributory factor to the observed difference.⁴⁰ The findings indicate that there has been a migration of the Al -ions/ ClO_4^- ions in opposite directions into/from the interior of the WO_3 nanoporosity, as stated by Forse et al.⁴¹ For the 0.5 M $\text{Al}(\text{ClO}_4)_3$ -PC electrolyte (Figure S5b), different kinds of ion exchange mechanisms are expected at different quantities of electric charges. Based on the value of the derivative of the plot of electrode mass change versus charge and the theoretical possibility (9 g/mol), the Al -ion electrolytes are classified into five broad types: cations deeply confined (region I), cation-dominated intercalation (region II), chelate-like compound-dominated intercalation (region III), chelate-like compound-dominated de-intercalation (region IV), and anion-dominated de-intercalation (region V). The experimental values of M/z in the five regions are summarized in Table S1. Starting from the zero charge ($\Delta Q = 0$), a different behavior is observed during region III and region IV where the electrode mass changes quickly. The fitted value is much larger than the theoretical possibility (9 g/mol) for regions III and IV at high ion concentrations, indicating the appearance of chelate-like compounds at the active interface of WO_3 /electrolyte. The mass change behavior at a low quantity of electric charge (-1.1 to -2.5 mC) is assigned to the dominant cation intercalation. Similarly, the values (1.4 – 2.7 mC) appear to support the assumption that the ClO_4^- anions are more inclined to reversibly intercalate and de-intercalate in the WO_3 thin film electrode at higher charge density, which are similar to those previously reported by Tsai et al.¹⁵ In region I, the mean slope of the experimental plot is close to that of the theoretical one due to the Al -ions deeply confined to the wider pores.²⁴ Hence, the most appropriate model for the mass change characteristic is two ideal ion exchange mechanisms in the WO_3 electrode, where cation exchange is dominant at low charge densities ($Q < 0$), and anion adsorption dominant processes can be manipulated at high charge densities ($Q > 0$). At the beginning of the electrochromic reaction, the existence of potential chelate-like compounds can inhibit these processes of intercalation and de-intercalation by destroying the SEI film, which can reduce the reversibility of the electrochemical reaction processes.

4. CONCLUSIONS

In summary, in situ real-time EQCM has been newly used for detecting the presence of chelate-like compounds in a novel Al -ion half-cell consisting of a WO_3 thin film cathode, an $\text{Al}(\text{ClO}_4)_3$ -PC electrolyte, and an Au counter electrode. The mass change of the WO_3 electrode has been directly measured by the in situ EQCM during the charge and discharge processes. The chelate-like compounds formation in the active interface of WO_3 /electrolyte has existed in high-concentration solutions instead of in low-concentration solutions. Quantitative resolution of the mass changes of the electroactive WO_3 electrode during cycling enables identification of a hitherto overlooked ion exchange mechanism. The chelate-like compounds reduces the stability of SEI and inhibits the process of intercalation and de-intercalation in the WO_3 thin film electrode. We anticipate the new findings and generated insight to be readily transferable to research in electrochemical

applications and, more generally, to the various ion intercalation hosts presently investigated for electrochemical energy storage and conversion applications.

■ ASSOCIATED CONTENT

Supporting Information

The Supporting Information is available free of charge at <https://pubs.acs.org/doi/10.1021/acsaem.1c03242>.

A table of the values of M/z ; SEM images and XRD patterns of the WO_3 thin film; EQCM results and analysis in different concentrations of electrolytes; TEM images of SEI; GCD curves under different experimental conditions (PDF)

■ AUTHOR INFORMATION

Corresponding Author

Hongliang Zhang – Laboratory of Advanced Nano Materials and Devices, Ningbo Institute of Materials Technology and Engineering, Chinese Academy of Sciences, Ningbo 315201, China; Center of Materials Science and Optoelectronics Engineering, University of Chinese Academy of Sciences, Beijing 100049, China; orcid.org/0000-0002-9295-8683; Email: zhanghl@nimte.ac.cn

Authors

Sheng Liu – Laboratory of Advanced Nano Materials and Devices, Ningbo Institute of Materials Technology and Engineering, Chinese Academy of Sciences, Ningbo 315201, China; Nano Science and Technology Institute, University of Science and Technology of China, Suzhou 215123, China

Xin Zhang – Laboratory of Advanced Nano Materials and Devices, Ningbo Institute of Materials Technology and Engineering, Chinese Academy of Sciences, Ningbo 315201, China

Qiang Wang – Ningbo Wakan Electronic Science Technology Co. Ltd., Ningbo 315475, China

Chengli Zhang – Ningbo Wakan Electronic Science Technology Co. Ltd., Ningbo 315475, China

Ran Jiang – School of Information Science and Engineering, Ningbo University, Ningbo 315211, China

Junhua Gao – Laboratory of Advanced Nano Materials and Devices, Ningbo Institute of Materials Technology and Engineering, Chinese Academy of Sciences, Ningbo 315201, China

Lingyan Liang – Laboratory of Advanced Nano Materials and Devices, Ningbo Institute of Materials Technology and Engineering, Chinese Academy of Sciences, Ningbo 315201, China; orcid.org/0000-0002-6285-6600

Hongtao Cao – Laboratory of Advanced Nano Materials and Devices, Ningbo Institute of Materials Technology and Engineering, Chinese Academy of Sciences, Ningbo 315201, China; Center of Materials Science and Optoelectronics Engineering, University of Chinese Academy of Sciences, Beijing 100049, China

Complete contact information is available at: <https://pubs.acs.org/doi/10.1021/acsaem.1c03242>

Author Contributions

The manuscript was written through contributions of all authors. All authors have given approval to the final version of the manuscript.

Notes

The authors declare no competing financial interest.

■ ACKNOWLEDGMENTS

This project is supported by the National Natural Science Foundation of China (61974148 and 61774098) and Ningbo Science and Technology Innovation 2025 Major Special Project (2020Z002).

■ REFERENCES

- (1) Shi, J.; Zhang, J.; Guo, J. Avoiding Pitfalls in Rechargeable Aluminum Batteries Research. *ACS Energy Lett.* **2019**, *4*, 2124–2129.
- (2) Tian, Y.; Zhang, W.; Cong, S.; Zheng, Y.; Geng, F.; Zhao, Z. Unconventional Aluminum Ion Intercalation/Deintercalation for Fast Switching and Highly Stable Electrochromism. *Adv. Funct. Mater.* **2015**, *25*, 5833–5839.
- (3) Lin, M. C.; Gong, M.; Lu, B.; Wu, Y.; Wang, D. Y.; Guan, M.; Angell, M.; Chen, C.; Yang, J.; Hwang, B. J.; Dai, H. An ultrafast rechargeable aluminium-ion battery. *Nature* **2015**, *520*, 325–328.
- (4) Li, H.; Firby, C. J.; Elezzabi, A. Y. Rechargeable Aqueous Hybrid $\text{Zn}^{2+}/\text{Al}^{3+}$ Electrochromic Batteries. *Joule* **2019**, *3*, 2268–2278.
- (5) Wang, L.; Guo, M.; Zhan, J.; Jiao, X.; Chen, D.; Wang, T. A new design of an electrochromic energy storage device with high capacity, long cycle lifetime and multicolor display. *J. Mater. Chem. A* **2020**, 17098.
- (6) Tripathi, A. M.; Su, W. N.; Hwang, B. J. In situ analytical techniques for battery interface analysis. *Chem. Soc. Rev.* **2018**, *47*, 736–851.
- (7) Ye, H.; Gui, S.; Wang, Z.; Chen, J.; Liu, Q.; Zhang, X.; Jia, P.; Tang, Y.; Yang, T.; Du, C.; Geng, L.; Li, H.; Dai, Q.; Tang, Y.; Zhang, L.; Yang, H.; Huang, J. In Situ Measurements of the Mechanical Properties of Electrochemically Deposited Li_2CO_3 and Li_2O Nanorods. *ACS Appl. Mater. Interfaces* **2021**, *13*, 44479–44487.
- (8) Zhao, R.; Wang, S.; Liu, D.; Liu, Y.; Lv, X.; Zeng, X.; Li, B. Effect of Fluoroethylene Carbonate on Solid Electrolyte Interphase Formation of the SiO/C Anode Observed by In Situ Atomic Force Microscopy. *ACS Appl. Energy Mater.* **2021**, *4*, 492–499.
- (9) Gao, W.; Krins, N.; Laberty-Robert, C.; Perrot, H.; Sel, O. Scrutiny of the LiCoO_2 Composite Electrode/Electrolyte Interface by Advanced Electrogravimetry and Implications for Aqueous Li-Ion Batteries. *J. Phys. Chem. C* **2021**, *125*, 3859–3867.
- (10) Dong, S.; Wu, L.; Xue, M.; Li, Z.; Xiao, D.; Xu, C.; Shen, L.; Zhang, X. Conductive Metal–Organic Framework for High Energy Sodium-Ion Hybrid Capacitors. *ACS Appl. Energy Mater.* **2021**, *4*, 1568–1574.
- (11) Kitz, P. G.; Novak, P.; Berg, E. J. Influence of Water Contamination on the SEI Formation in Li-Ion Cells: An Operando EQCM-D Study. *ACS Appl. Mater. Interfaces* **2020**, *12*, 15934–15942.
- (12) Cora, S.; Ahmad, S.; Sa, N. In Situ Probing of Mass Exchange at the Solid Electrolyte Interphase in Aqueous and Nonaqueous Zn Electrolytes with EQCM-D. *ACS Appl. Mater. Interfaces* **2021**, *13*, 10131–10140.
- (13) Sauerbrey, G. Use of oscillator quartz crystals for weighing thin layers and microweighing. *Z. Phys.* **1959**, *155*, 206.
- (14) Buttry, D. A.; Ward, M. D. Measurement of interfacial processes at electrode surfaces with the electrochemical quartz crystal microbalance. *Chem. Rev.* **1992**, *92*, 1355–1379.
- (15) Tsai, W. Y.; Taberna, P. L.; Simon, P. Electrochemical quartz crystal microbalance (EQCM) study of ion dynamics in nanoporous carbons. *J. Am. Chem. Soc.* **2014**, *136*, 8722–8728.
- (16) Janz, G. J.; Ambrose, J.; Coutts, J. W.; Downey, J. R. Raman spectrum of propylene carbonate. *Spectrochim. Acta* **1979**, *35*, 175–179.
- (17) Battisti, D.; Nazri, G. A.; Klassen, B.; Aroca, R. Vibrational studies of lithium perchlorate in propylene carbonate solutions. *J. Phys. Chem.* **1993**, *97*, 5826–5830.
- (18) Zhang, B.; Zhou, Y.; Li, X.; Wang, J.; Li, G.; Yun, Q.; Wang, X. $\text{Li}(+)$ -molecule interactions of lithium tetrafluoroborate in propylene carbonate + N,N -dimethylformamide mixtures: an FTIR spectroscopic study. *Spectrochim. Acta, Part A* **2014**, *124*, 40–45.
- (19) Zhang, B.; Yuan, Z.; Xiang, L.; Ren, X.; Qiang, Y. Ion-molecule Interaction in Solutions of Lithium Tetrafluoroborate in Propylene Carbonate: an FTIR Vibrational Spectroscopic Study. *Int. J. Electrochem. Sci.* **2013**, *8*, 12735–12740.
- (20) Verma, V.; Chan, R. M.; Jia Yang, L.; Kumar, S.; Sattayaporn, S.; Chua, R.; Cai, Y.; Kidkhunthod, P.; Manalastas, W.; Srinivasan, M. Chelating Ligands as Electrolyte Solvent for Rechargeable Zinc-Ion Batteries. *Chem. Mater.* **2021**, *33*, 1330–1340.
- (21) Razzaghi, F.; Debiemme-Chouvy, C.; Pillier, F.; Perrot, H.; Sel, O. Ion intercalation dynamics of electrosynthesized mesoporous WO_3 thin films studied by multi-scale coupled electrogravimetric methods. *Phys. Chem. Chem. Phys.* **2015**, *17*, 14773–14787.
- (22) Komayko, A. L.; Ryazantsev, S. V.; Trussov, I. A.; Arkharova, N. A.; Presnov, D. E.; Levin, E. E.; Nikitina, V. A. The Misconception of Mg^{2+} Insertion into Prussian Blue Analog Structures from Aqueous Solution. *ChemSusChem* **2021**, 1574.
- (23) Platek-Mielczarek, A.; Frackowiak, E.; Fic, K. Specific carbon/iodide interactions in electrochemical capacitors monitored by EQCM technique. *Energy Environ. Sci.* **2021**, *14*, 2381–2393.
- (24) Fedorov, M. V.; Kornyshev, A. A. Ionic Liquid Near a Charged Wall: Structure and Capacitance of Electrical Double Layer. *J. Phys. Chem. B* **2008**, *112*, 11868–11872.
- (25) Verma, P.; Maire, P.; Novák, P. A review of the features and analyses of the solid electrolyte interphase in Li-ion batteries. *Electrochim. Acta* **2010**, *55*, 6332–6341.
- (26) Melato, A. I.; Mendonça, M. H.; Abrantes, L. M. Effect of the electropolymerisation conditions on the electrochemical, morphological and structural properties of PEDOT films. *J. Solid State Electrochem.* **2009**, *13*, 417–426.
- (27) Gupta, B.; Singh, A. K.; Prakash, R. Electrolyte effects on various properties of polycarbazole. *Thin Solid Films* **2010**, *519*, 1016–1019.
- (28) Wang, Z.; Chen, G.; Zhang, H.; Liang, L.; Gao, J.; Cao, H. In situ TEM investigation of hexagonal WO_3 irreversible transformation to Li_2WO_4 . *Scr. Mater.* **2021**, *203*, 114090.
- (29) Borodin, O.; Ren, X.; Vatamanu, J.; von Wald Cresce, A.; Knap, J.; Xu, K. Modeling Insight into Battery Electrolyte Electrochemical Stability and Interfacial Structure. *Acc. Chem. Res.* **2017**, *50*, 2886–2894.
- (30) Peled, E. The Electrochemical Behavior of Alkali and Alkaline Earth Metals in Nonaqueous Battery Systems—The Solid Electrolyte Interphase Model. *J. Electrochem. Soc.* **1979**, *126*, 2047–2051.
- (31) Katorova, N. S.; Luchkin, S. Y.; Rupasov, D. P.; Abakumov, A. M.; Stevenson, K. J. Origins of irreversible capacity loss in hard carbon negative electrodes for potassium-ion batteries. *J. Chem. Phys.* **2020**, *152*, 194704.
- (32) Luchkin, S. Y.; Lipovskikh, S. A.; Katorova, N. S.; Savina, A. A.; Abakumov, A. M.; Stevenson, K. J. Solid-electrolyte interphase nucleation and growth on carbonaceous negative electrodes for Li-ion batteries visualized with in situ atomic force microscopy. *Sci. Rep.* **2020**, *10*, 8550.
- (33) Zhao, N.; Yang, Y.; Xiao, Y.; Wang, C.; Ha, M. N.; Cui, W.; Wang, X. Unveiling the SEI layer formed on pillar-structured MXene anode towards enhanced Li-ion storage. *Scr. Mater.* **2021**, *202*, 113988.
- (34) Guo, J.; Guo, X.; Sun, H.; Xie, Y.; Diao, X.; Wang, M.; Zeng, X.; Zhang, Z. B. Unprecedented Electrochromic Stability of $\alpha\text{-WO}_{3-x}$ Thin Films Achieved by Using a Hybrid-Cationic Electrolyte. *ACS Appl. Mater. Interfaces* **2021**, *13*, 11067–11077.
- (35) Luo, K.; Wang, D.; Chen, D.; Zhong, Y.; Zheng, Z.; Wang, G.; Liu, Y.; Zhong, B.; Wu, Z.; Guo, X. Solid Electrolyte Interphase Composition Regulation via Coating AlF_3 for a High-Performance Hard Carbon Anode in Sodium-Ion Batteries. *ACS Appl. Energy Mater.* **2021**, *4*, 8242–8251.
- (36) Santiago, A.; Castillo, J.; Garbayo, I.; Saenz de Buruaga, A.; Coca Clemente, J. A.; Qiao, L.; Cid Barreno, R.; Martinez-Ibañez, M.; Armand, M.; Zhang, H.; Li, C. Salt Additives for Improving

Cyclability of Polymer-Based All-Solid-State Lithium–Sulfur Batteries. *ACS Appl. Energy Mater.* **2021**, *4*, 4459–4464.

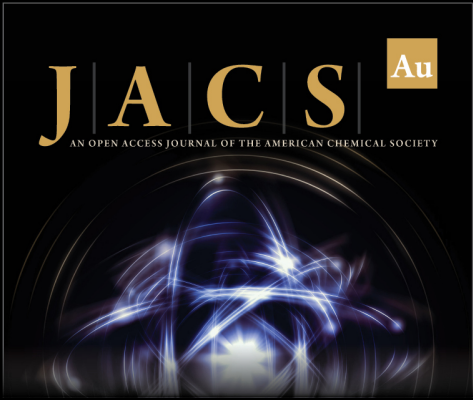
(37) Dargel, V.; Shpigel, N.; Sigalov, S.; Nayak, P.; Levi, M. D.; Daikhin, L.; Aurbach, D. In situ real-time gravimetric and viscoelastic probing of surface films formation on lithium batteries electrodes. *Nat. Commun.* **2017**, *8*, 1389.

(38) Huggins, R. A.; Nix, W. D. Decrepitation model for capacity loss during cycling of alloys in rechargeable electrochemical systems. *Ionics* **2000**, *6*, 57–63.


(39) Zhang, H.; Liu, S.; Xu, T.; Xie, W.; Chen, G.; Liang, L.; Gao, J.; Cao, H. Aluminum-ion-intercalation nickel oxide thin films for high-performance electrochromic energy storage devices. *J. Mater. Chem. C* **2021**, *9*, 17427–17436.


(40) Yamagata, S.; Takahara, I.; Wang, M.; Mizoguchi, T.; Yagi, S. EQCM analysis of intercalation species into graphite positive electrodes for Al batteries. *J. Alloys Compd.* **2020**, *846*, 156469.

(41) Forse, A. C.; Merlet, C.; Griffin, J. M.; Grey, C. P. New Perspectives on the Charging Mechanisms of Supercapacitors. *J. Am. Chem. Soc.* **2016**, *138*, 5731–5744.




JACS Au
AN OPEN ACCESS JOURNAL OF THE AMERICAN CHEMICAL SOCIETY

 Editor-in-Chief
Prof. Christopher W. Jones
Georgia Institute of Technology, USA

Open for Submissions 

pubs.acs.org/jacsau

 **ACS Publications**
Most Trusted. Most Cited. Most Read.